Nigerian Journal of Physics (NJP)
ISSN online: 3027-0936
ISSN print: 1595-0611
DOI: https://doi.org/10.62292/njp.v34i3.2025.417
Volume 34(3), September 2025

In Silico Investigations of the Performance Characteristics of Agbis$_2$ Solar Cell using Solar Cell Capacitance Simulator – 1 Dimension (SCAPS-1D)

*[1,2]Olopade, M. A., [2]Swaray, S. and [2]Feika, A. M.

[1]Department of Physics, University of Lagos, Nigeria.
[2]Department of Physics, Fourah Bay College, University of Sierra Leone, Sierra Leone.

*Corresponding author: Email: molopade@unilag.edu.ng

ABSTRACT

The research presents a theoretical investigation of a layered structure of ITO/ZnO/$AgBiS_2$/Spiro OMeTAD/MoO_3/Ag of $AgBiS_2$ photovoltaic cells. The top layer is composed of indium tin oxide (ITO) as a window layer, while intrinsic ZnO serves as the electron transport layer (ETL), a p-type $AgBiS_2$ absorber layer followed by two distinct hole-transport layers (HTLs), namely spiro-OMeTAD and molybdenum trioxide (MoO_3) and (Ag) serving as the back contact. This study aims to examine the effects of Spiro-OMeTAD HTL on the efficiency of an $AgBiS_2$-based heterostructure solar cell. The consequences of optimising various parameters, such as absorber thickness, absorber defect density, molybdenum trioxide (MoO_3) thickness, and temperature on the device efficiency were studied. The initial model achieved an efficiency of 9.62%, further enhanced to 11.86% by incorporating MoO_3 as a secondary hole transport layer. Optimising the MoO_3 thickness yielded a peak efficiency of 12.40%. Increasing the absorber thickness led to improved light absorption and carrier generation, with the highest performance of 14.16% achieved at 200 nm. Defect density variations from 10^{10} to 10^{20} cm^{-3} had a minimal impact on device performance, indicating the device's resilience to moderate defect changes. Temperature studies revealed an optimal operating range below 310 K, with the highest efficiency of 15.34% obtained at 280 K. These findings provide valuable understanding into the potential of $AgBiS_2$-based solar cells and the key parameters for performance optimisation. Hence, the device's resilience to moderate defect changes and the importance of temperature management for maximising the efficiency of $AgBiS_2$-based solar cells.

Keywords: Spiro-OMeTAD, $AgBiS_2$, Defect density, Temperature, Photovoltaic.

INTRODUCTION

Significant efforts are being made to develop efficient energy materials and novel conversion technologies to replace fossil fuels in response to the growth in global energy demand and the quest for clean, safe, and reliable energy sources (Ma et al., 2022). Although challenging to capture, sunlight is arguably the most abundant and sustainable clean energy source (Shiyani et al., 2021). Developing environmentally friendly and renewable energy sources is a primary goal for scientists and researchers worldwide to reduce the negative impacts of CO_2 emissions, such as coal, oil, and natural gas, caused by burning fossil fuels, to generate electricity (Azam et al., 2023; Maka & Alabid, 2022). Photovoltaics are among the essential forms of clean energy for meeting the growing energy demand and advancing green energy (Kabir et al., 2018). Solar energy has the greatest potential to satisfy future energy demands. These cells harness solar radiation via photoconductivity to generate electrical energy (Huen & Daoud, 2017). Within the framework of solar technology, the pursuit of novel materials suitable for photovoltaic energy conversion has emerged as a crucial area of investigation. $AgBiS_2$ (ABS), or silver bismuth sulfide, toxic-free, can be considered a greener, safer energy alternative for sustainable applications with promising semiconductor materials composition for photovoltaic (PV) (Bernechea et al., 2016). An efficiency of 7.3% has recently been demonstrated for solution-processed mixed ABS (Burgués-Ceballos et al., 2022). An analytical study has reported a Photovoltaic Conversion Efficiency of 26% for PV cells based on ABS (Akhil & Balakrishna, 2022).

This thin-film $AgBiS_2$ solar cell device with an area of 0.06 cm^2 achieved a conversion efficiency (PCE) of 10% using a vapour-assisted solution method (Li et al., 2024). Furthermore, under regular worldwide sunshine conditions of 100 mW/cm^2 (Air Mass 1.5), the efficiency was 9.53% for a greater active surface of 1.00 cm^2 (Kim et al., 2022). These efficiencies are the highest reported thus far and are becoming increasingly interesting to scientists as potential thermoelectric materials and absorbers for thin-film solar cells. $AgBiS_2$ is well suited for thin-film solar cell applications owing to its reduced energy band gap between 1.2 and 1.3 eV and a higher absorption coefficient (~ $10^5 cm^{-1}$) (Pai et al., 2018) (Zdanowicz et al., 2005). Further advances in its use could reveal information about its thermoelectric, optoelectronic, photovoltaic, and structural properties. Despite the promising features of $AgBiS_2$ perovskite solar cells, including low manufacturing costs and broad-spectrum light absorption, their application has been hindered by their low power conversion efficiency (PCE), poor stability, and low charge carrier mobility (Green, 2016). Numerical modelling can significantly improve the efficiency of silver bismuth sulfide-based devices by optimising their structural and electronic characteristics. The purpose of this study is to demonstrate the possible improvement of the efficiency of the $AgBiS_2$ solar cell through the enhancement of the various parameters of the device structure.

MATERIALS AND METHODS

Computational Details

The SCAPS-1D (Solar Cell Capacitance Simulator – 1 Dimension) software was used to model and analyse the performance of silver bismuth sulfide solar cells. A layered structure is proposed for the thin-film solar cell: ITO/ZnO/$AgBiS_2$/Spiro-OMeTAD/MoO_3/Ag. Each layer's role is specified, including the use of two separate hole transport layers. The solar cell was simulated under standard illumination conditions (AM1.5G, 100 mW/cm2) at an operational temperature of 300 K. Input parameters for each layer, such as electron and hole mobility, optical band gap and electron affinity, were taken from previous reports (Kashem & Esha, 2025). Work functions for the back (Ag) and front (ITO) contacts were set to specific values based on the employed electron and hole thermal velocity values. The parameters used for all layers in the base model are listed in Table 1. The relationship between potential and space charges was described by Poisson's equation, as shown in Equation 1and the free electrons and holes carrier concentrations are expressed by Equations 2 and 3 (Burgelman et al., 2000).

$$\varphi(x) = [n(x) - p(x) - N_D + (x) + N_A - (x) - p_t(x) + n_t nt\,(x) \quad (1)$$

$$n = N_c exp(E_f - \frac{E_c}{K_{BT}} \quad (2)$$

$$p = N_v exp(E_v - \frac{E_f}{K_{BT}} \quad (3)$$

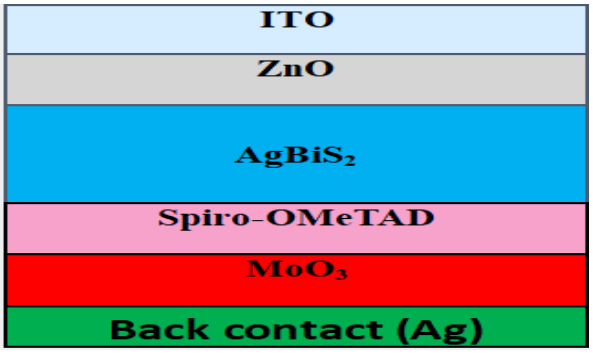

Figure 1: An illustrative configuration of the suggested $AgBiS_2$ thin-film solar cell (ITO/ZnO/$AgBiS_2$/Spiro–OMeTAD/MoO_3/Ag)

Table 1: Available Experimental and Theoretical Values Used in the Simulation Processes (Banik Et Al., 2024;Sayeem Et Al., 2024; Sultan Et Al., 2024)

Parameters	MoO_3	Spiro-OMeTAD	$AgBiS_2$	ZnO	ITO
Thickness (nm)	100	180	300	80	60
Bandgap (eV)	1.7	1.5	1.3	3.3	3.6
Electron affinity (eV)	4.2	4.5	4.5	4.6	4.1
Dielectric permittivity	13.6	10	10	9	10
CB effective density of states (cm^{-3})	2.2×10^{18}	2.2×10^{18}	2.2×10^{18}	2.2×10^{18}	2.2×10^{18}
VB effective density of states (cm^{-3})	1.8×10^{19}	1.8×10^{19}	1.8×10^{19}	1.8×10^{18}	1.8×10^{19}
Electron thermal velocity (cm s^{-1})	1×10^7	1×10^7	1.8×10^7	1×10^7	1×10^7
Hole thermal velocity (cm^{-1})	1×10^7	1×10^7	1×10^7	1×10^7	1×10^7
Electron mobility (cm2/VJ)	100	100	100	100	50
Hole mobility (cm2/Vs)	25	25	25	25	75

Parameters	MoO_3	Spiro-OMeTAD	$AgBiS_2$	ZnO	ITO
Shallow uniform donor density, ND (cm^{-3})	0	1×10^{1}	5×10^{15}	1×10^{18}	1×10^{19}
Shallow uniform acceptor density, Nu (cm^{-3})	1×10^{16}	1.9×10^{14}	1×10^{1}	0	0
Defect type	-	Donor	Acceptor	-	-
Defect density (cm^{-3})	-	1×10^{13}	1×10^{16}	-	-

RESULTS AND DISCUSSION

The efficiency of a solar cell is significantly affected by the absorption coefficient of the semiconducting material used. A standard SCAPS optical absorption model was used to plot the variations in the absorption coefficients of the Electron transport layers (ETL), absorber layers, and Hole transport layers (HTL), as shown in Figure 2. Figure 3 shows an illustration of the Energy Band Alignment of the Simulated Device Structure of the suggested structure with potential optical transitions. The first stage of this simulation examines and presents the performance of the base model of ITO (60 nm), ZnO (80 nm), $AgBiS_2$ (300 nm), Spiro-OMeTAD (180 nm), with a further incorporation of MoO_3 (100 nm) as the secondary hole transport layer and Ag (back contact). Thereafter, the photovoltaic cell performance parameters were obtained from the current-voltage (J-V) characteristics of the photovoltaic cell, wherein Voc = 0.7624V, Jsc = 15.569163 (mA/cm^2), FF = 81.06%, and eta = 9.62%. The resulting current-voltage characteristic (J-V) plot is shown in Figure 4.

Absorption Coefficient for ETL, Absorber, and HTL Layers

The graph shows how the optical absorption coefficient (α) changes with photon energy for different layers: ZnO (ETL), $AgBiS_2$ (absorber), Spiro OMeTAD (HTL), and MoO_3 (HTL). The $AgBiS_2$ absorber layer has a high electromagnetic radiation over a broad range of wavelengths, especially in the visible range. This means that it can absorb sunlight well and create electron-hole pairs. ZnO (ETL) has a broad bandgap and doesn't absorb much light in the visible spectrum, which means that most photons can reach the absorber (Wibowo et al., 2020). Its main job is to move electrons, not to absorb light. Spiro OMeTAD and MoO_3 (HTLs) don't absorb much light in the visible range, which helps keep the material clear and stops photon loss while still allowing for good hole transport. The strong absorption of $AgBiS_2$ compared to the other layers shows that it is the best at collecting light. The ETLs and HTLs make sure that charge transmission is efficient without losing too many photons (Jobsis et al., 2024).

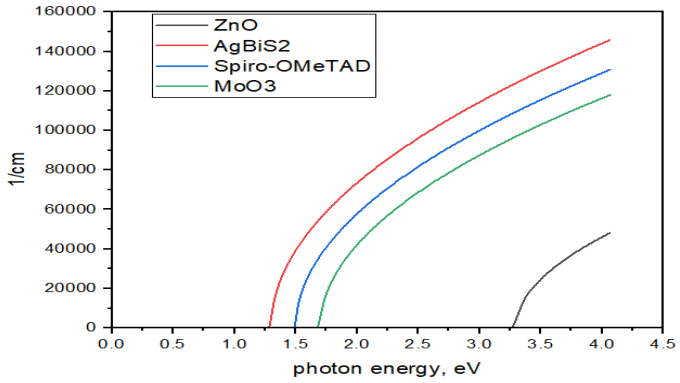

Figure 2: Plot showing the absorption coefficient of ETL, CPs Absorber, and HTLs Layers

Aligning the Energy Bands of the $AgBiS_2$ Solar Cell Device Structure

This energy level explains how the different energy levels, such as the band of electrons, valence band, and Fermi levels, are distributed across different layers. This helps to explain possible optical transitions and charge transport paths. The conduction band minimum (CBM) of Zinc oxide and $AgBiS_2$ is very close to each other, which makes it simple for electrons to get into the electron transport layer (ETL). At the same time, the valence band maximum (VBM) of $AgBiS_2$ lines up with Spiro OMeTAD and MoO_3. This helps with hole extraction and creates an energy gradient that reduces recombination losses. MoO_3 has a high work function, which makes holes more selective and reduces electron backflow. This improves overall charge separation. (Xiao et al., 2021). This staggered band alignment keeps energy losses to a minimum during charge transport, which raises the Voc and FF. The way the cell device parts are aligned with each other creates a cascade structure that makes it easier to selectively and efficiently extract charge while preventing recombination.

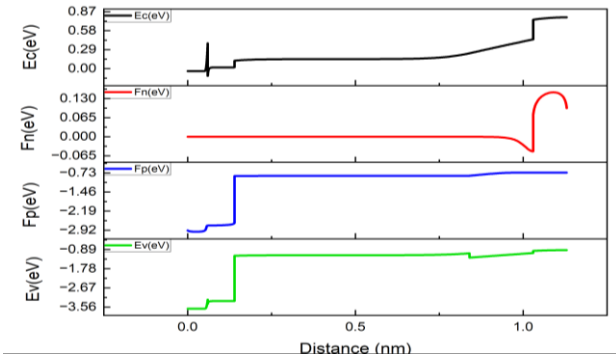

Figure 3: Energy Band Alignment of the Device Structure

J V Curve for the Proposed $AgBiS_2$ Device

The J-V graph under conventional lighting circumstances (AM1.5G, 100 mW/cm²) gives us important information about how well the device works as a solar cell. This curve shows an important solar cell metric (These et al., 2024). At zero volts, the current density is the same as Jsc, which is caused by photo-generated carriers that are pulled through the contacts. At Voc, the current drops to zero because the built-in electric field cancels out the movement of carriers. The fill factor (FF) measures how square the curve is, which shows how much energy is lost through resistance and recombination in the device (Zhang et al., 2025). The total efficiency (η) is based on how well absorbed photons are turned into electrical power. The graph shows that the device separates and moves charges efficiently, with very little loss due to recombination. The Voc, Jsc, and FF values are all rather high, which means that $AgBiS_2$-based solar cells could be very efficient.

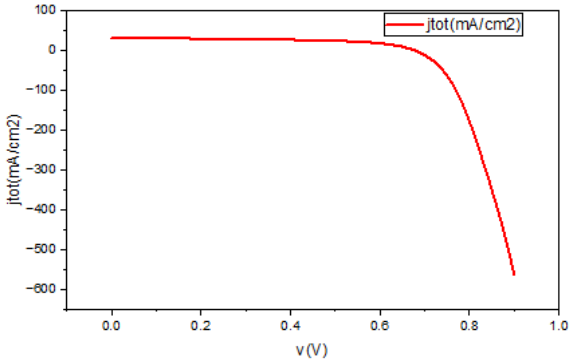

Figure 4: J-V curve of the suggested $AgBiS_2$ Solar Cell.

Impact of MoO_3 as a Secondary Hole Transport Layer

After presenting the characteristics of the base model with an efficiency of 9.62%, we also incorporated MoO_3 as a secondary hole transport layer (HTL). Using two HTLs can increase the effectiveness of charge carrier extraction by generating an energy gradient that promotes hole transport. Energy loss can be decreased by combining materials with varying energy levels to improve alignment with the active layer. One HTL can enhance device performance by passivating flaws or surface traps at interfaces. By shielding delicate layers from deterioration, using two materials can improve the stability of solar cells. A very efficient hole transport layer (HTL) in photovoltaic cells is molybdenum trioxide (MoO_3) (Avigad & Etgar, 2018). Its wide bandgap guarantees optical transparency and its strong work function for effective hole extraction and energy alignment with active materials (Nakamura et al., 2015). In our work, MoO_3 serves as the secondary HTL, increasing device thermal and chemical stability along with efficiency and decreasing recombination losses and improving charge selectivity (Zeinidenov et al., 2021). However, issues like moisture sensitivity and processing costs must be resolved to realise its full potential. This implies that introducing MoO_3 as a secondary HTL is essential for balancing the absorption and carrier transport in solar devices and serves as a passivation layer. Incorporating MoO_3 as the second hole-transport layer further enhanced the device performance, with an efficiency of 11.86%.

Impact of MoO_3 Layer Thickness Optimization on Device Performance.

After incorporating MoO_3 as secondary hole transport layer, the study further optimizes its thickness by varying it from 10nm –100nm to examine the effects of important photovoltaic parameters on short-circuit current density (Jsc), open-circuit voltage (Voc), fill factor (FF), and efficiency (eta), the result is presented in Figure 5. As the thickness increased, the short-circuit current density (Jsc) marginally decreased, suggesting that an increased thickness could result in larger optical losses or lower carrier collection efficiency. First, the open-circuit voltage (Voc) reveals a slight increase in thickness before stabilising at higher thickness levels. This might be due to a reduction in recombination effects at optimal thickness levels. A thinner HTL results in low shunt resistance and current leakage, which results in a lower Fil factor (FF) (Lin et al., 2019). Hence, an increase in the MoO_3 results in a decrease in the fill factor. The combined effects of reduced Jsc, FF, and limited improvement in Voc caused the total efficiency to decline as the thickness increased. In this case, thinner layers appear to be more effective. In our work, fine-tuning the thickness of MoO_3 is essential for effectively extracting holes, preventing electron flow, aligning energy levels, reducing recombination, and safeguarding the active layer, which in turn enhances the solar cell's efficiency, stability, and longevity. This implies that thickness optimisation is essential for balancing the absorption and carrier transport in solar devices. It can be inferred that variation of the thickness of the MoO_3 layer further enhanced the solar cell performance, with Jsc = 35.628271mA/cm^2, Voc = 0.6784073 V, FF = 58.32%, and PCE = 12.40% respectively.

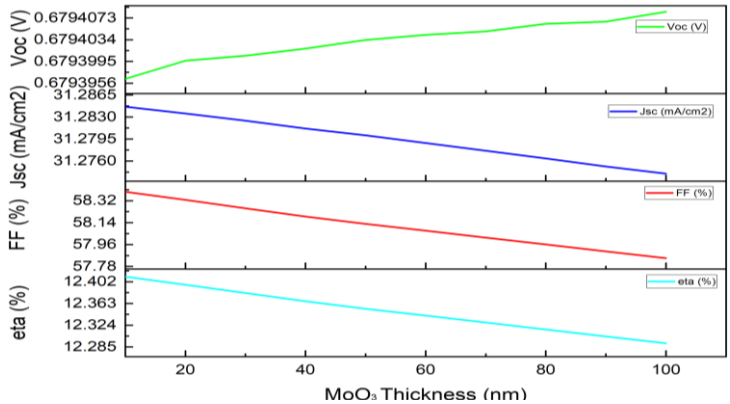

Figure 5: Presents Plots for the Variation of MoO_3 Thickness Optimization on Device Parameters

Device Performance with Variation of $AgBiS_2$ Layer Thickness

The thickness of the absorber layer ($AgBiS_2$) has a direct impact on the properties of the device, as revealed in Figure 6, making it a critical design factor for photovoltaic cells. Hitherto, the absorber layer is where electron-hole pair formation takes place (Chang et al., 2019). Increasing the thickness of the absorber layer results in electron-hole pair generation aided by higher incident light absorption (Schwartz et al., 2020). Voc increases slightly as the absorber thickness increases, indicating better charge carrier generation (Abdelaziz et al., 2020). With thicker layers, and increases almost linearly between 60 nm and 300 nm, starting at approximately 0.6878 V at 60 nm and increasing to 0.6935 V at 300 nm. Short-circuit current Density (Jsc) fluctuates but generally trends upward with increasing thickness and fluctuates with peaks and dips, increasing from 35.75 mA/cm² at 60 nm to a peak around 36 mA/cm² near 200 nm, then dropping slightly at 300 nm. This suggests an enhanced light absorption and carrier collection to a certain level of thickness (Tan et al., 2016). Fill factor (FF) decreased with increasing thickness and decreased steadily from approximately 57.42% at 60 nm to 57.13% at 300 nm. This may result from the higher series resistance in thicker layers or recombination losses. The efficiency (eta) shows minor variations but generally remains stable. The highest efficiency was achieved at a specific thickness to a peak of approximately 14.16% near 200 nm, balancing the absorption and recombination effects.

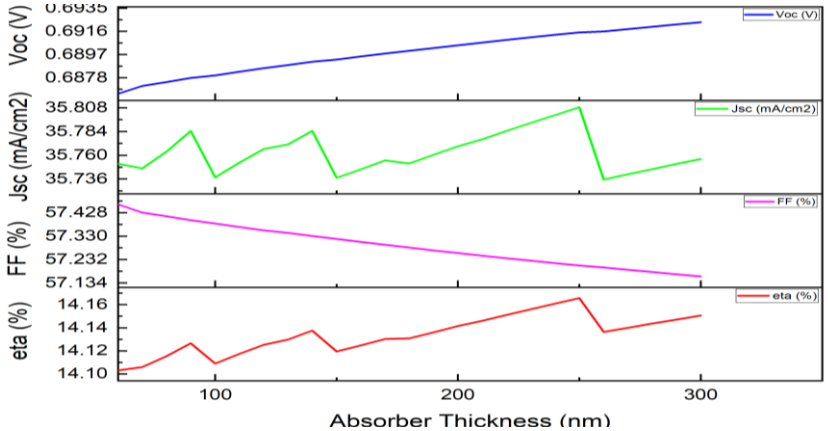

Figure 6: Illustrates the impact of absorber layer thickness on device parameters

Effect of Variation of Absorber Layer Defect Densities

Defects in the system may alter optoelectronic characteristics. The effect of the defect density (Nt) on the performance characteristics of photovoltaic metrics is depicted in Figure 7. The defect density ranged from 1010 to 1020 $cm^{-3,}$ and only a modest rise in the short-circuit current density (Jsc) was observed when the defect density increased. Because defect-related recombination losses do not predominate in charge generation, this suggests that Jsc is not significantly affected by defect density within this range (Chouhan et al., 2018). Across the defect density range, the open-circuit voltage (Voc) essentially stays constant. This shows that the recombination processes that normally affect Voc are not significantly affected by an increase in the defect density. Additionally, the fill factor (FF) has a very slight increasing tendency and is essentially unaffected by defects, suggesting that even when defect density (Nt) varies, the processes of charge transport and extraction remain constant. In our simulations, even though a higher defect density might not have a big impact on open-circuit voltage (OCV) and fill factor (FF), it can actually enhance ionic conductivity and possibly alter the electronic band structure. As the defect density increased, the efficiency (eta) also marginally increased (Et-taya et al., 2020). This implies that the device continues to operate steadily and that the alterations do not substantially impair photovoltaic performance within this range of defect densities. The defect density had a negligible consequence on the solar cell performance metrics (Jsc, FF, Voc and eta) in the range under analysis. The device performance remains stable across a wide range of defect densities because $AgBiS_2$ is a highly tolerant electronic material with strong ionic bonding and self-compensating defects. Its electronic band structure minimises the negative effects of recombination centres and suppresses non-radiative recombination pathways. This indicates that the device can withstand moderate changes in defect density, most likely owing to efficient defect passivation or the predominance of other mechanisms over recombination caused by defects (Jamal et al., 2019). The device performance remains stable at different defect densities, and an efficiency (eta) of 14.15% was obtained by optimising the defect density to 1 x 10^{10} cm^3 in the absorber ($AgBiS_2$).

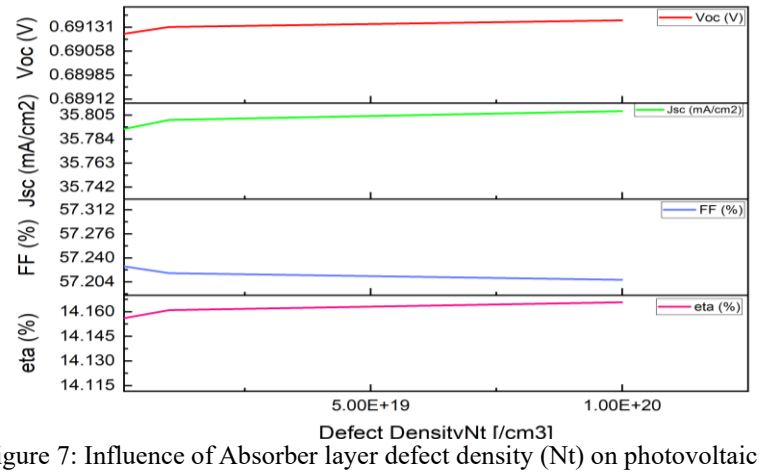

Figure 7: Influence of Absorber layer defect density (Nt) on photovoltaic parameters

Impact of Operating Temperature

Following the absorber layer defect density optimization, we investigated additional performance enhancements by adjusting the working temperature from 280 K to 345 K. As the temperature rises over about 310 K, the efficiency falls. This is a typical finding for PV devices because higher temperatures lower the open-circuit voltage and fill factor, which lowers the overall efficiency. Moreover, the combined behaviour of Voc and Jsc determines (Singh & Ravindra, 2012). The efficiency seems to be steady below 310 K, suggesting that this is the temperature range in which the device operates at its best. The fill factor remains constant at lower temperatures but increases significantly at 310 K and peaks close to this temperature. However, when the temperature increased above 315 K, it decreased. This behaviour may result from temperature influences that affect the PV cell resistance and charge transport. A decrease in the open circuit voltage is observed with a rise in temperature. The semiconductors' band gap energy decreases with an increase in temperature of the PV cell, and the charged particles' velocity-instability increases, reversing the materials' resistivity and saturation current and lowering Voc is expected in PV devices (Varshni, 1967) (Alam & Ashraf, 2024). A crucial thermal threshold is highlighted by the abrupt drop at 310-315 K; the current density is comparatively constant, but as the temperature increases above 315 K, it begins to decrease drastically. The reduced carrier mobility or higher recombination rates at higher temperatures may cause this decrease (Khattak et al., 2018). Observations have shown that the performance of $AgBiS_2$-based solar cells was temperature-sensitive, with the highest efficiency of about 15.34% achieved at 280 K. Maintaining operating temperatures below 310 K is crucial for maximising device performance, underscoring the need for temperature management in practical applications. We observe that although performance experiences a slight decline at elevated temperatures, the optimisation of thermal stability through materials engineering—such as enhanced encapsulation and the development of heat-resistant transport layers—can effectively sustain efficiency in hot climates. Findings are presented in Figure 8.

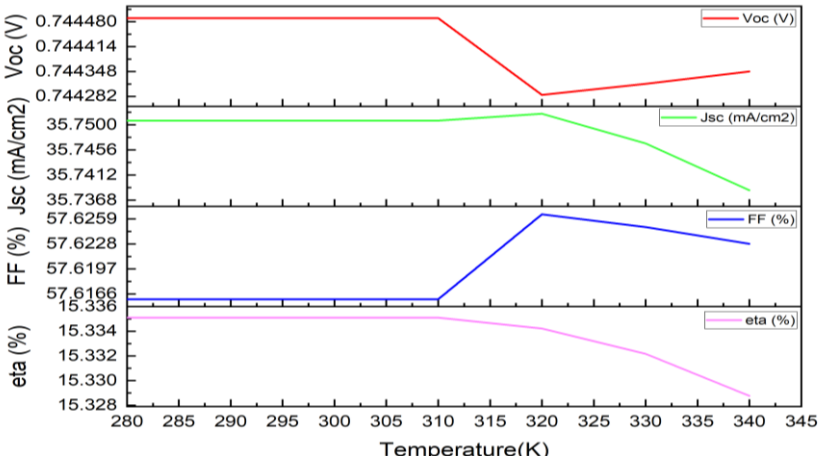

Figure 8: The impact of operating Temperature on photovoltaic parameters

CONCLUSION

The enhancement of $AgBiS_2$-based solar cells was successfully carried out with Solar Cell Capacitance Simulator – 1 Dimension (SCAPS-1D) numerical modelling software. A layered structure (ITO/ZnO/$AgBiS_2$/Spiro-OMeTAD/MoO_3/Ag) was proposed and optimised, showing significant efficiency improvements. The initial model efficiency of 9.62% was improved to 15.34% through various optimisations, including the addition of MoO_3 as a secondary hole transport layer, and adjustments to layer thicknesses and operating temperature. $AgBiS_2$ demonstrated high tolerance to defects, maintaining stable performance across a wide range of defect densities. The study identified an optimal operating temperature range below 310 K, with peak performance at 280 K. The research findings provided valuable insights into the key parameters and design considerations for enhancing the efficiency of $AgBiS_2$-based solar cells, informing and guiding future research in this area. The findings highlight the potential of $AgBiS_2$-based PV cells and the key parameters for performance optimisation.

ACKNOWLEDGMENT

We appreciate Prof. Marc Burgelman and his group at the University of Ghent for granting access to SCAPS-1D (Solar Cell Capacitance Simulator – 1 Dimension) software for this research.

REFERENCES

Abdelaziz, S., Zekry, A., Shaker, A., & Abouelatta, M. (2020). Investigating the performance of formamidinium

tin-based perovskite solar cell by SCAPS device simulation. *Optical Materials*, *101*, 109738. https://doi.org/10.1016/j.optmat.2020.109738

Alam, I., & Ashraf, M. A. (2024). Effect of different device parameters on tin-based perovskite solar cell coupled with In2S3 electron transport layer and CuSCN and Spiro-OMeTAD alternative hole transport layers for high-efficiency performance. *Energy Sources, Part A: Recovery, Utilisation, and Environmental Effects*, *46*(1), 17080–17096. https://doi.org/10.1080/15567036.2020.1820628

Avigad, E., & Etgar, L. (2018). Studying the Effect of MoO_3 in Hole-Conductor-Free Perovskite Solar Cells. *ACS Energy Letters*, *3*(9), 2240–2245. https://doi.org/10.1021/acsenergylett.8b01169

Banik, S., Das, A., Das, B. K., & Islam, N. (2024). Numerical simulation and performance optimization of a lead-free inorganic perovskite solar cell using SCAPS-1D. *Heliyon*, *10*(1), e23985. https://doi.org/10.1016/j.heliyon.2024.e23985

Chang, W., Tian, H., Fang, G., Guo, D., Wang, Z., & Zhao, K. (2019). Simulation of innovative high efficiency perovskite solar cell with Bi-HTL: NiO and Si thin films. *Solar Energy*, *186*, 323–327. https://doi.org/10.1016/j.solener.2019.05.017

Jobsis, H. J., Gao, L., Reponen, A.-P. M., VanOrman, Z. A., Rijpers, R. P. P. P. M., Wang, H. I., Feldmann, S., & Hutter, E. M. (2024). *The Effect of Charge Carrier Cooling on the Ultrafast Carrier Dynamics in Cs$_2$AgBiBr$_6$ Thin Films* (Version 1). arXiv. https://doi.org/10.48550/ARXIV.2412.14929

Kashem, M. T. B., & Esha, S. A. (2025). *A Comprehensive Computational Photovoltaic Study of Lead-free Inorganic NaSnCl$_3$-based Perovskite Solar Cell: Effect of Charge Transport Layers and Material Parameters* (Version 1). arXiv. https://doi.org/10.48550/ARXIV.2503.02845

Khattak, Y. H., Baig, F., Ullah, S., Marí, B., Beg, S., & Ullah, H. (2018). Enhancement of the conversion efficiency of a thin-film kesterite solar cell. *Journal of Renewable and Sustainable Energy*, *10*(3), 033501. https://doi.org/10.1063/1.5023478

Lin, L., Jiang, L., Li, P., Qiu, Y., & Yan, Q. (2019). Numerical analysis of inverted-structure perovskite solar cell based on all-inorganic charge transport layers. *Journal of Photonics for Energy*, *9*(02), 1. https://doi.org/10.1117/1.JPE.9.024501

Nakamura, M., Nakamura, H., Ohsawa, T., Imura, M., Shimamura, K., & Ohashi, N. (2015). AgBiS2 single crystal grown using slow cooling method and its characterization. *Journal of Crystal Growth*, *411*, 1–3. https://doi.org/10.1016/j.jcrysgro.2014.10.042

Sayeem, S. A., Siddika, Mst. A., Basu, S. R., Mondal, B. K., & Hossain, J. (2024). Numerical Expedition on the Potential of $AgBiS_2$ -Based Thin Film Solar Cells Employing Different Carrier Transport Layers. *ACS Omega*, *9*(33), 35490–35502. https://doi.org/10.1021/acsomega.4c02375

Schwartz, D., Murshed, R., Larson, H., Usprung, B., Soltanmohamad, S., Pandey, R., Barnard, E. S., Rockett, A., Hartmann, T., Castelli, I. E., & Bansal, S. (2020). Air Stable, High-Efficiency, Pt-Based Halide Perovskite Solar Cells with Long Carrier Lifetimes. *Physica Status Solidi (RRL) – Rapid Research Letters*, *14*(8), 2000182. https://doi.org/10.1002/pssr.202000182

Singh, P., & Ravindra, N. M. (2012). Temperature dependence of solar cell performance—An analysis. *Solar Energy Materials and Solar Cells*, *101*, 36–45. https://doi.org/10.1016/j.solmat.2012.02.019

Sultan, Md. Z., Shahriar, A., Tota, R., Howlader, Md. N., Rodro, H. H., Akhy, M. J., & Rashik, Md. A. A. (2024). Numerical Study and Optimization of CZTS-Based Thin-Film Solar Cell Structure with Different Novel Buffer-Layer Materials Using SCAPS-1D Software. *Energy and Power Engineering*, *16*(04), 179–195. https://doi.org/10.4236/epe.2024.164009

Tan, K., Lin, P., Wang, G., Liu, Y., Xu, Z., & Lin, Y. (2016). Controllable design of solid-state perovskite solar cells by SCAPS device simulation. *Solid-State Electronics*, *126*, 75–80. https://doi.org/10.1016/j.sse.2016.09.012

These, A., Koster, L. J. A., Brabec, C. J., & Le Corre, V. M. (2024). Beginner's Guide to Visual Analysis of Perovskite and Organic Solar Cell Current Density–Voltage Characteristics. *Advanced Energy Materials*, *14*(21), 2400055. https://doi.org/10.1002/aenm.202400055

Varshni, Y. P. (1967). Temperature dependence of the energy gap in semiconductors. *Physica*, *34*(1), 149–154. https://doi.org/10.1016/0031-8914(67)90062-6

Wibowo, A., Marsudi, M. A., Amal, M. I., Ananda, M. B., Stephanie, R., Ardy, H., & Diguna, L. J. (2020). ZnO nanostructured materials for emerging solar cell applications. *RSC Advances*, *10*(70), 42838–42859. https://doi.org/10.1039/D0RA07689A

Xiao, Y., Wang, H., Awai, F., Shibayama, N., Kubo, T., & Segawa, H. (2021). Eco-Friendly $AgBiS_2$ Nanocrystal/ZnO Nanowire Heterojunction Solar Cells with Enhanced Carrier Collection Efficiency. *ACS Applied Materials & Interfaces*, *13*(3), 3969–3978. https://doi.org/10.1021/acsami.0c19435

Zeinidenov, A., Mukametkali, T., Ilyassov, B., Aimukhanov, A., & Valiev, D. (2021). The effect of MoO3 interlayer on electro-physical characteristics of the perovskite solar cells. *Synthetic Metals*, *281*, 116903. https://doi.org/10.1016/j.synthmet.2021.116903

Zhang, H., Xia, Y., Zhang, Y., Ghorpade, U. V., He, M., Shin, S. W., Hao, X., & Suryawanshi, M. P. (2025). The Rise of Chalcohalide Solar Cells: Comprehensive Insights From Materials to Devices. *Advanced Science*, *12*(19), 2413131. https://doi.org/10.1002/advs.202413131